OPEN JOURNAL SISTEMS
ISSN:2237-2202

Available on line at Directory of Open Access Journals

Journal of Hyperspectral Remote Sensing v.04, n.05 (2014) 121-128

Journal of Hyperspectral Remote Sensing
www.ufpe.br/jhrs

Application of non-negative ICA for unmixing of Hyperion data

Majid Mohammady Oskouei[1], Rashed Poormirzaee[2]
[1] Faculty of Mining Engineering, Sahand University of Technology, Tabriz, Iran, E-mail: mohammady@sut.ac.ir
[2] Faculty of Mining Engineering, Sahand University of Technology, Tabriz, Iran, E-mail: Rashed.poormirzaee@gmail.com
[**] ***Corresponding author. Email:*** mohammady@sut.ac.ir

Received 22 November 2014; received in revised from 28 November 2014: accepted 30 November 2014.

A B S T R A C T

Independent Component Analysis (ICA) is based on the linear mixture model of hyperspectral data and has been widely used in various blind source separations. Non-negative ICA considers non negativity constraint in addition to independency of components and the results will therefore be more real because negative signal sources in an image are not physically meaningful. The non-negative Independent Component Analysis (ICA) was used for detection and mapping of endmembers on a Hyperspectral dataset in this study. This paper surveys the capability of non-negative ICA for endmember detection and unmixing of Hyperion data in a geological terrain. In this research, a small part of the Hyperion scene was processed using the geodesic search algorithm to distinguish the Independent Components (ICs) of the image. The dataset was first topographically and atmospherically corrected and then data quality assessment was performed for recognizing the bad bands. The applied method for unmixing was able to detect the major minerals in the study scene and resulted in more accurate outcome in comparison to regular ICA. The non-negative ICA algorithm satisfactory identified three ICs, of which one showed considerable abundances in the region. The determined minerals are also more compatible to the geology and lithological features in the region. It therefore can map alterations and minerals abundances with higher accuracy. The abundances map of detected minerals was generated using spectral angle mapper method that proved as a useful tool for this purpose.

Keywords: hyperspectral, Hyperion, non-negative ICA, unmixing

1 Introduction

Hyperspectral Imagery is a developing technique that a large number of studies have been conducted to apply and/or improve the related processing algorithms. Such a considerable interest is due to their high-quality and accurate information about the Earth surface, which are available in different wavelengths. Hyperspectral imaging has been recently emerged as a very interesting area in the remote sensing topics. Many applications of statistical signal processing techniques to Hyperspectral imaging have been documented in Wang and Chang 2006a.

The use of Hyperspectral imaging sensor to study the Earth's surface is based on the capability of such sensors to provide hundreds of spectral bands (high resolution spectra), providing one spectrum per pixel, along with the image data. This capability can be used to determine the constituent signatures of the Earth from the spectral information provided by the sensor (Martinez et al. 2006).

Independent Component Analysis (ICA) is based on the linear mixture model of hyperspectral data and has been widely used in various blind source separations. Its application to linear spectral mixture analysis in remote sensing and image processing has shown promising results (Oskouei 2010). The basic idea is to decompose a set of multivariate signals in to a basis of statistically independent sources with minimal loss of information content so as to achieve detection and unmixing (Du et al. 2006). Non-negative ICA considers non negativity constraint in addition to independency of components. This constraint will result in more real outcomes because negative signal sources in an image are meaningless.

Hyperspectral unmixing is the decomposition of the pixel spectral into a collection of constituent spectra, or spectral signatures, and their corresponding fractional abundance that indicates the proportion of each endmember present in the pixel (Keshava and Mustard

2002). Observation signals are determined using Equation 1:

$$X=AS \tag{1}$$

Where S is source signals which can be positive and independent, A is demixing matrix, and X is observations signals.

Considering the non-negative ICA concept, the matrix A can be obtained using the concept of geodesic search on the manifold of orthonormal matrixes. This algorithm can perform separation quickly. Some non-negative ICA algorithm requires a preliminary sphering or whitening of the data (Oskouei 2010). There are a small number of studies about unmixing of Hyperspectral data using the non-negative ICA algorithm for geological surveys. This study aims to unmix Hyperion data of the Syahroud region located at the north-west of Iran using non-negative ICA.

1.1 Study Area

The Syahroud area is located 70 km west of Ahar in the north-west of Iran. The area geologically comprises of Eocene volcanic rocks as andesit, dasite, volcanic breccia, basic tuff, and synsedimentary volcanic rocks. Post Eocene magmatism has had an active role in shaping the geology of the Syahroud area, which its results can be seen as Oligocene plutonism and volcanic activities.

Syahroud is located between 46˚ 00' and 46˚ 30' E and 38˚ 00' and 38˚ 30' N. Due to our limitations in undertaking this research in a large area, approximately 7 Km2 of Hyperion image was only selected for processing purposes. This area is located between 46 14' 33" and 46 10' 2"E and 38 31' 40" and 38 30' 20" N (Figure 1). The intrusion of Oligocene parts in various facieses has caused different alterations and mineralization such as copper, molybdenum, gold, and iron, in the study area.

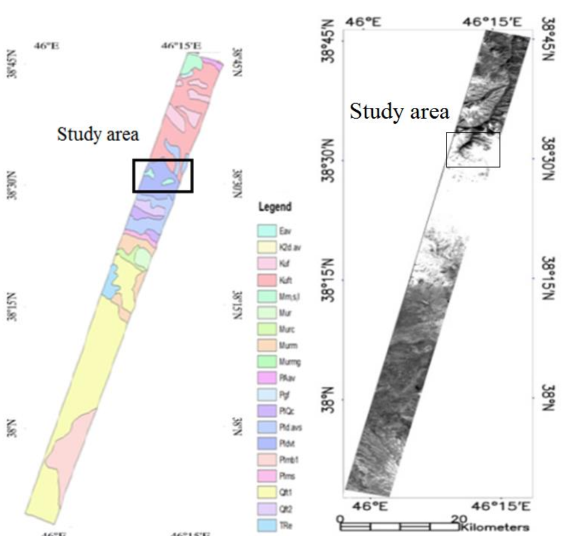

Figure 1: The location of the study area (Mehrpartov 1997)).

1.2 Hyperion description

The objective of the Hyperion instrument is to provide high quality calibrated data that can support evaluation of Hyperspectral technology for Earth observing missions. Hyperspectral images can be defined as images with a high spectral resolution, typically 100 to 300 different wavelengths (Riaño et al. 2003). The Hyperion is a pushbroom instrument and each image frame taken in this "pushbroom" configuration captures the spectrum of a line 30 m long by 7.5 km wide (perpendicular to the satellite motion). Frames are then combined to form a two dimensional spatial image with a complete spectral signature for each pixel. Hyperion has a single telescope and two spectrometers, visible/near infrared (VNIR) and short-wave infrared (SWIR) spectrometers (covering spectral range from 0.4 to 2.5 µm). Each pixel views a 30 × 30 m region of the ground. The swath length of each image depends on the duration of the collect and is commanded by the spacecraft (Soenen et al. 2005).

1.3 Pre-processing

There is a preprocessing stage dealing with data errors before the main processing concerning on the sensor type and its technical specifications. The pre-processing includes algorithms to correct probable errors that occur during image acquisition (Oskouei 2010).

The atmospheric and topographic corrections and quality assessment are performed on the Hyperion data. To compensate undesirable effect resulting from atmospheric and electromagnetic interaction, the implementation of the atmospheric correction is necessary. The conversion of radiance to reflectance is the main goal of the atmospheric correction. There are a number of algorithms developed for the atmospheric correction, such as ATREM, FLAASH, ATCOR, and ACORN. The atmospheric correction was performed on data used in this study, using the Fast Line-of-sight Atmospheric Analysis of Spectral Hypercubes (FLAASH). The FLAASH calculates the apparent reflectance based on the MODTRAN code, accommodates for pixel adjacency errors, and spectrally polishes output values.

The topographic correction, or topographic normalization, refers to the compensation of different solar illuminations due to the irregular shape of the terrain (Riaño et al. 2003). This effect causes a high variation in the reflectance response for same type objects. As seen in Figure 2, the shaded area shows lees reflectance than expected, while the sunny area is truly reflected.

The topographic correction of remotely sensed imagery received considerable attention in the early 1980s through the development of a variety of photometric technique. These methods were applied and tested in various studies (Soenen et al. 2005). These methods mainly included Cosine Correction, Minnaert Correction, Statistical-Empirical Correction, and C-Correction.

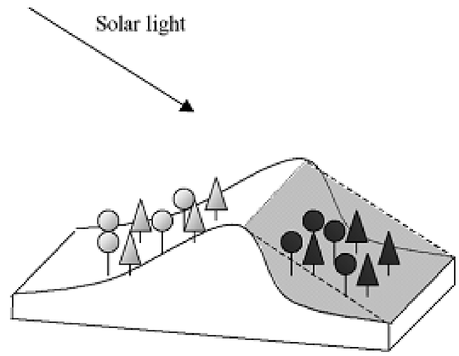

Figure 2: Topographic effects on reflectance.

Among others, the C-correction approach has shown its reliability for the topographic correction (Teillet et al. 1982; Meyer et al. 1993; Riaño et al. 2003; Soenen et al. 2005). In this study, the C-correction method was used to reduce the topographically induced variations in the reflectance (LT). The topographic correction is determined using Equation 2:

$$LH = LT\,\frac{(\cos(\theta_i)+c)}{(\cos\gamma_i+c)} \qquad (2)$$

Where LH is the reflectance observed for a normal surface and θ_i is the solar zenith angle. The solar incidence angle, IL, is calculated using Equation 3:

$$I_L = \cos\gamma_i = \cos\theta_p\cos\theta_i + \sin\theta_i\sin\theta_p\cos(\varphi_a - \varphi_0) \quad (3)$$

Where θ_p is the terrain surface slope, φ_a is the solar azimuth angle and φ_0 is the slope aspect (Figure 3). The slope and aspect are obtained using a Digital Elevation Model (DEM). The parameter is determined using the linear regression analysis:

$$L_T = a\cos(i) + b\,,\, c = \frac{b}{a} \qquad (4)$$

The stepwise process of topographic correction using the C-correction method is summarized as follows:
Entrance of Hyperion imagery
Calculation of IL using Equation 3.
Calculation of the regression between I_L and nth Hyperion bands using Equation 4.

Calculation of Normalized Reflectance for each bands of Hyperion using Equation 2.

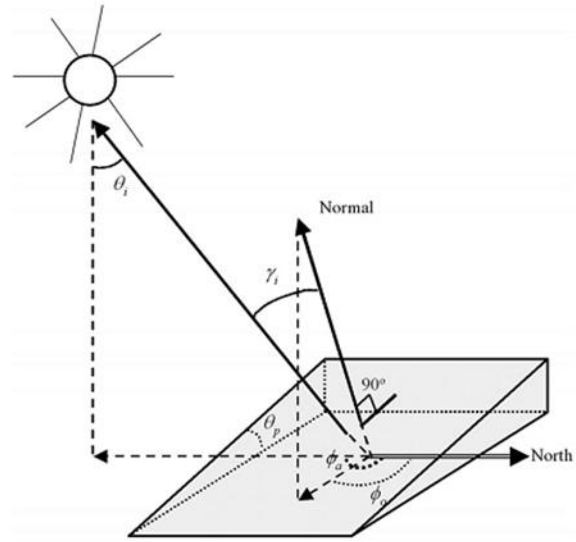

Figure 3: Angles involved in the computation of IL.

Equations 1- 4 were coded in the interactive data language (idl) using the c-correction algorithm, the lh was calculated for each band of hyperion. once the atmospheric and topographic corrections were performed, the quality of data was assessed. this process smoothens noisy fluctuations on spectral profile, and small absorption features are probably eliminated. therefore, bands that have very little or no extractable information in this task are retrenched. the quality of digital remote sensing data is directly related to the level of the signal to noise ratio (snr) (oskouei 2010).
one common approach for determining an approximate snr for remote sensing data is to use a mean/standard deviation method. this approach requires definition of a spectrally homogeneous area (an area with minimum intrinsic variance), calculation of the average spectrum for that area, and determination of the spectrally distributed standard deviation for the average spectrum (manolakis et al. 2003).

Figure 4 illustrates the signal to noise ratio calculated for our hyperion data using the abovementioned method. as seen in this plot, bands that possess lower snr ratio compared to the nearby channels are considered to be bad bands. it should be mentioned that the un-calibrated channels (channels 1-8 and 222-242) were previously eliminated. after this stage, only 142 good bands were selected to perform unmixing task on the data.

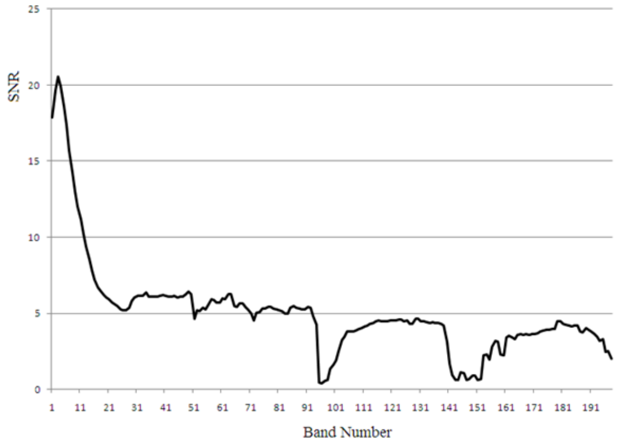

Figure 4: SNR plot of the data.

2 Non-negative ICA

In many practical applications of remote sensing image analysis, it may be very difficult or even impossible to get prior information about class signatures, so unsupervised methods need to be applied (Du et al. 2006). Hyperspectral sensors have demonstrated the capability of performing spectral unmixing where several hundred spectral bands are collected. In Hyperspectral imagery, mixed pixels are a mixture of more than one distinct substance, and they exist for one of two reasons. First, if the spatial resolution of a sensor is low enough that disparate materials can jointly occupy a single pixel, the resulting spectral measurement will be some composite of the individual spectra. Second, mixed pixels can result when distinct materials are combined into a homogeneous mixture. This circumstance can occur independent of the spatial resolution of the sensor (Keshava and Mustard 2002).

In general, The ICA problem can often be simplified if the data is white

$$C_X = E((X - \bar{X})(X - \bar{X})^T) = I \quad (5)$$

where $\bar{X}$ is the mean of X (Plumbley 2003). The whitening program of FastICA package was run to whiten Hyperion imagery. To have a successful attempt of unmixing, the Virtual Dimensionality (VD) of the dataset was then determined using the HFC method (Harsanayi et al. 1993). This is equal to the theoretical number of detectable endmembers. The HFC method is introduced by Harsanyi et al. 1993 and uses the Neyman-Pearson detection theory to estimate the number of endmembers (Chang and Du 2004). The application of the HFC algorithm yielded the VD of the data set as 22.

In non-negative ICA problems, it suffices to find an orthonormal rotation weight matrix, W, for which $W^TW=WW^T=I_n$ is satisfied and Y=WX (X is whitening data) is independent (Plumbley 2003). Typical ICA algorithms search for an extreme of a contrast function, which are expressed as either higher-order cumulates or non-linear cross-terms between outputs (Hyvarinen et al. 2001). Suppose that the vector of source s is an n-dimensional random vector of real-valued and non-negative sources. And let the components of s be well-grounded, meaning that they have a non-zero probability density function (pdf) in the positive neighbourhood of s=0, i.e. for any $\delta>0$ we have $Pr(s<\delta)>0$. Then, the outputs vector y is a permutation of the source if and only if all the output components of y are non-negative with probability 1. This means that if we ensure that all of the output components are non-negative, then we will have found the set independent sources (subject to scaling and permutation) (Plumbley 2003).

A natural way to do this is to construct a cost function J (W), for which J=0 if and only if y is non-negative with probability 1. Then finding the zero point of this cost function will also find the independent sources. Specifically, we can choose the squared-reconstruction-error cost function

$$J=J_2(W)=1/2(E|x-\hat{x}|^2) \quad (6)$$

Where $\hat{x}=W^TY^+$ and Y^+ is the rectified version of Y=WX. Thus, it suffices to find an orthonormal weight matrix W that minimizes the mean squared reconstruction error J (Plumbley 2003).

2.1 Steepest-descent geodesic

One particular concept that offers the potential for fast batch methods for the non-negative ICA is that of the geodesic: the shortest path between two points on a manifold (Edelman et al. 1998). We restrict our consideration to the case n=m of square matrices W. in this case, the geodesic equation takes the simple form (Zheng et al. 2006)

$$W(\tau)=e^{\tau B}W(0) \quad (7)$$

Where B is n×n skew-symmetrical (B^T= -B) and τ is a scalar parameter determining the position along the geodesic (Plumbley 2003). We wish to construct an algorithm which, at each step, searches over a geodesic for the minimum of J. The geodesic is chosen in the direction of the steepest descent, i.e. the one for which J is decreasing fastest for a given small distance moved (Plumbley 2003).

Consider Eq 5, where we write $B=\Phi-\Phi^T$ for an underlying upper-triangular parameter matrix $\Phi=[\emptyset_{ij}]$, constrained such that $\emptyset_{ij}$ for i<j are the free parameters, with $\emptyset_{ij}=0$ for i≥j. For the steepest descent direction, we wish to choose Φ which maximizes the expression:

$$\lim_{\delta_{\tau\to 0}} \frac{(\text{change in } J(\tau\Phi)\text{due to } \delta_\tau)/\delta_\tau}{(\text{distance moved by of } \tau\Phi \text{ due to } \delta_\tau)/\delta_\tau} \quad (8)$$

To construct a steepest gradient descent algorithm, we would simply move it by a small amount in the steepest descent direction, generating a small multiplicative update step for W:

$$W(t+1) = e^{-\eta(Y_- Y_+^T - Y_+ Y_-^T)} W(t) \quad (9)$$

Equation 8 is a direct application of the geodesic flow method (Plumbley 2003).

Now we can perform a line search to find the minimum for J along this geodesic.

A repeating line search algorithm to perform this is presented below:

1) X (0) =X and W(0) =I at step t=0.
2) Calculate Y=X (t) =W(t)X(0).
3) Calculate the gradient G(t) = UT ($Y_- Y_+^T - Y_+ Y_-^T$) and B-space movement direction H(t) = - (G (t) – $G(t)^T$) = $Y_- Y_+^T - Y_+ Y_-^T$.
4) Stop if $\|G(t)\| < tolerance$.
5) Perform a line search for τ^*which minimizes J (τ) using Y(τ) =R(τ)X(τ) and R (τ) =$e^{-\tau H}$.
6) Update w(t+1)=R(τ^*)W(t) and X(t+1)=R(τ^*)X(t)=W(t+1)X(0).
7) Increment t, repeat from 2. Until exit at 4.

Where $\|G(t)\|$ is the Frobenius norm.

The above algorithm was programmed in Matlab, and examined for different predefined tolerances. This threshold is the smallest amounts that the algorithm be converged in a reasonable time. Therefore, the convergence of the algorithm was achieved after several iterations and the demixing matrix was computed. Multiplication of this matrix by original data will result in non-negative ICs images.

3 Unmixing of the data

Unmixing of the data and mapping of ICs abundances for the FastICA results was already introduced by Zheng et al. 2006 and Wang and Chang 2006b, and improved by Oskouei 2010. For each endmember pixel $e_{i,}$, let IC_i be the IC from which e_i was extracted and $IC_i(r)$ denote the value of each pixel r in IC_i. We normalized the absolute value of $IC_i(r)$, $|IC_i(r)|$ with respect to $|e_i|$, the absolute value of e_i and define its corresponding abundance fraction $a_{ICi}(r)$ by

$$a_{ICi}(r) = \frac{|IC_i(r)| - \min_r |IC_i(r)|}{|e_i| - \min_r |IC_i(r)|} \quad (10)$$

Where e_i is the maximum of $|IC_i(r)|$ over all the image pixels in the IC_i .

In each channel of this image, the location of any pixel that had a maximum amount for the appropriate IC was determined. Knowing the location of such a pixel would help to preliminary evaluate non-negative independent components and their similarities. In addition, the images of each IC were verified surveyed visually to find the ICs that are related to backgrounds. The results demonstrate that some of the IC images have the same extreme pixel meaning that their maximum amount occurred in the same pixels, like ICs 3, 8, 32, 124 and ICs 55,120,95,27,97,114. The priority score for each IC band was then calculated using the method introduced by Wang and Chang [2006b]. We then calculated the priority scores for the ICs channels, and determined one IC as a representative for each group according to their priority score (22 ICs).

$$ps(IC_i) = \frac{(k_i^3)^2}{12} + \frac{(k_i^4 - 3)^2}{48} \quad (11)$$

Where $k_i^3 = \frac{\sum_{n=1}^{MN} (Z_{n=1}^i)^3}{MN}$, $k_i^4 = \frac{\sum_{n=1}^{MN} (z_n^i)^4}{MN}$ and Z_n^i is the DN of Pixel n in IC_i.

The ICs are listed in Table 1 along with their priority scores.

The spectral profiles of these 22 ICs were surveyed and compared with each other. Eight ICs were therefore detected that their extreme pixels are listed in Table 2. The mineralogy of those ICs as unknown spectra were then compared to The USGS mineral spectral library as reference spectra using by spectral analyst tool available on ENVI. Spectral Feature Fitting (SFF) and Spectral Angle Mapper (SAM) methods on the tool were applied to compute a similarity score between unknown and reference spectra. The similarity between an IC and reference spectral profiles were also surveyed visually to achieve reliable accuracy mostly considering the location of absorption features (Figure 5). The resultant minerals for each IC are also illustrated in table 2.

Table1: The priority of all ICs

52	51	53	69	38	47	30	20	31	18	33	40	23	28	49	63	19	48	42	14	22	16	8
21	54	12	68	29	46	32	50	45	41	26	70	43	6	39	15	7	17	67	2	9	13	10
44	11	88	57	24	4	66	3	56	72	35	25	1	36	55	58	133	64	27	34	74	86	59
5	87	61	62	132	37	83	78	139	76	60	73	79	80	71	77	75	65	113	105	106	129	136
82	114	107	81	94	96	131	90	93	95	84	98	100	101	119	85	111	108	89	112	92	109	117
125	120	124	126	102	135	99	138	140	128	122	118	110	121	123	103	91	130	104	97	137	127	116
115	134	141																				

Table 2: The location of ICs

No.	X	Y	IC
1	22	138	38
2	28	39	53
3	16	168	110
4	1	103	52
5	19	67	31
6	1	46	111
7	11	115	55
8	18	51	69

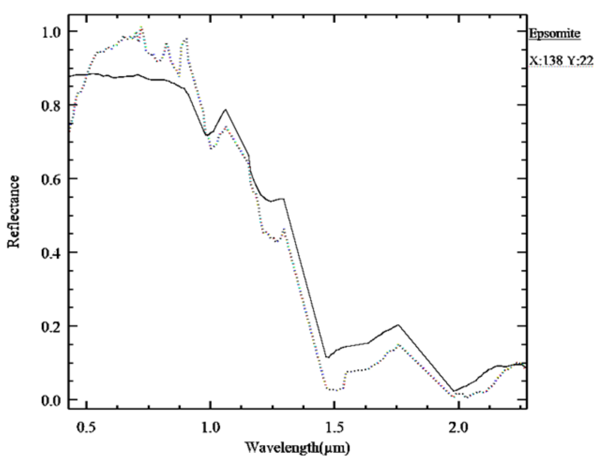

Figure 5: an example of comparison of an ICA spectra with reference spectrum (epsomite)

The non-negative ICA advantage to ordinary ICA and its overall performance was evaluated by running the same processing on the ENVI ICA. The resultant ICs and respected minerals are presented in table 3. The number of detected minerals in this algorithm decreased to three as many of the ICs are repetitive. The non-negative ICA therefore, was able to distinguish more endmembers. Its functionality to better endmember detection, and considering its non-negativity base which is more realistic, the presented algorithm in this study is more effective for mineral detection studies.

Table 3: detected minerals for the respected ICs by the ENVI ICA.

Mineral	IC
Manganitie	1
Epsomite	2
Epsomite	3
Kainite	4
Epsomite	5
Epsomite	6
Ulexite	7
Ulexite	8

The SAM Classifier was then used to identify the ICs distribution on the study area. The results show that the distribution of IC38 is considerably more than others on this map (Figure 6). The resultant map is reasonable given the small size of the study area and location and extension of geological exposures. It is worth noting that IC38 is representative of 47 of ICs, showing the most number of ICs represented by one IC. The classification of ICs based on their maximum presence in the image pixels (rule classifier method), however, implied a different distribution pattern (Figure 7). Since the study area is small and has few geological features, the map generated using the SAM classifier is closer to geological knowledge of the area compared to the map resulted from the rule classifier.

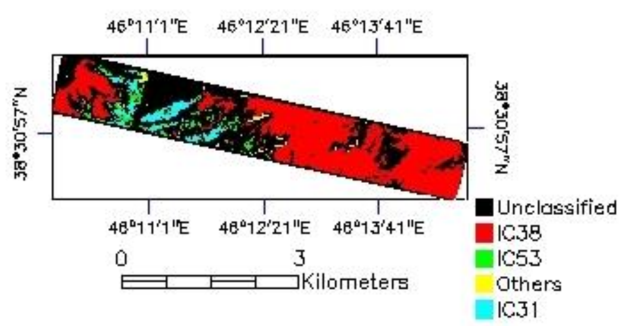

Figure 6: The ICs distribution map using the SAM method.

The method for abundance mapping of ICs is done as following step by step algorithm (Oskouei 2010) :

1) Change non-negative ICs images to an abundances map using Eq 9
2) Find the maxima for each non-negative IC (extreme pixels)

3) Group the non-negative ICs with the same extremes
4) Prioritization
5) Select one IC for each group based on their priority score
6) Classify the dataset using the SAM based on the extremes' spectral profiles

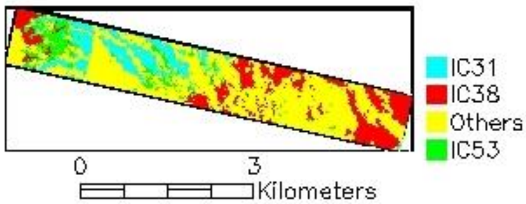

Figure 7: The ICs distribution map using the Rule classifier method.

4 Conclusion

Unmixing of Hyperspectral imagery is the main purpose in Hyperspectral remote sensing. The accuracy of the resultant map of the study area was directly depended on detection and determination of endmembers and an accurate estimation of their abundances. Non-negative ICA, as a new method in the image processing, was applied on a Hyperion image in this study to evaluate its functionality upon ordinary ICA. Non-negative ICA seems to be more meaningful than similar methods it solely processes positive signals. This fact was revealed in this study as non-negative ICA was able to detect more minerals in the region than the ENVI ICA. The determined minerals are also more compatible to the geology and lithological features in the region (Mehrpartov 1997). Therefore, it can be potentially used to map alterations and minerals with higher accuracy. The reliable functionality of the SAM method was also proved as a useful tool for mapping of resultant ICs.

References

Chang C.I., Du Q., 2004: Estimation of number of spectrally distinct signal source in hyperspectral imagery. – IEEE Transaction on Geoscience and Remote Sensing, 42: 608-619.

Du Q., Kopriva I., Szu H., 2006: Independent component analysis for hyperspectral remote sensing imagery classification. – Optical Engineering, 45(1): 017008. DOI:10.1117/1.2151172.

Edelman A., Arias T.A., Smith S.T., 1998: The geometry of algorithms with orthogonality constraints. – SIAM Journal on Matrix Analysis and Applications, 20: 303-353.

Harsanyi J.C., Farrand W., Chang C.I., 1993: Determining the number and identity of spectral endmembers: an integrated approach using Neyman-Pearson eigenthresholding and iterative constrained RMS error minimization. – Proc. of 9th Thematic Conference of Geologic Remote Sensing, California, USA., pp. 395-408.

Hyvarinen A., Karhunen J., Oja E., 2001:Independent Component Analysis. – John Wiley & Sons, pp. 247.

Keshava N., Mustard J., 2002: Spectral unmixing. IEEE Signal Processing Mag, 19: 44-57.

Manolakis D., Marden D., Shaw G.A., 2003: Hyperspectral image processing for automatic target detection application. – Lincoln Laboratory Journal, 14: 79-166.

Martinez P., Perez R.M., Plaza A., Aguilar PL., Cantero M.C., Plaza J., 2006: Endmember extraction algorithms from hyperspectral images. – Annals of Geophysics, 49(1): 93-101.

Mehrpartov M., 1997: 1:100000 Geological Map and geological report of Siahrood. – Geological Survey of Iran.

Oskouei M.M., 2010: Independent component analysis of Hyperion data to map alteration zones. – Journal of photogrammetry, remote sensing and geoinformation processing (PFG), 2010/3: 179-189. DOI: 10.1127/1432-8364/2010/0048.

Plumbley M., 2003: Algorithm for non-Negative Independent Component Analysis. – IEEE Transactions on Neural Networks, 14: 534 – 543.

Riaño D., Chuvieco E., Salas J., Aguado I., 2003: Assessment of different topographic corrections in Landsat-TM data for mapping vegetation types. – IEEE Transactions on Geoscience and Remote sensing, 41(5): 1056-1061.

Soenen S.A., Peddle D.R., Coburn C.A., 2005: A modified sun-canopy-sensor topographic correction in forested terrain. – IEEE Transactions on Geoscience and Remote Sensing, 43(9): 2148-2159.

Wang J., Chang C.I., 2006: Independent component analysis with application in hyperspectral image analysis. – IEEE Trasaction on Geoscience and Remote Sensing, 44: 1586-1600.

Wang J., Chang CI., 2006: Applications of Independent Component Analysis (ICA) in endmember extraction and abundance quantification for hyperspectral imagery. – IEEE Transactions on Geoscience & Remote Sensing, 44(9): 2601-2616

Zheng C.H., Huang D.S., Sun Z.L., Lyu M.R., Lok T.M., 2006: Nonnegative independent component analysis based on minimizing mutal information technique. – Neuro Computting, 69: 878-883.